

## Photochemical Studies of Alkylammonium Molybdates. Part 8.† Location of Protons interacting with the Paramagnetic Electron in a Single Crystal of Photoirradiated $[\text{NH}_3\text{Pr}^i]_6[\text{Mo}_8\text{O}_{26}(\text{OH})_2]\cdot 2\text{H}_2\text{O}‡$

Toshihiro Yamase\* and Masanobu Suga

Research Laboratory of Resources Utilization, Tokyo Institute of Technology, 4259 Nagatsuta, Midori-ku, Yokohama 227, Japan

The e.s.r. spectrum of a photoirradiated single crystal of  $[\text{NH}_3\text{Pr}^i]_6[\text{Mo}_8\text{O}_{26}(\text{OH})_2]\cdot 2\text{H}_2\text{O}$  at room temperature reveals the interaction of two magnetically equivalent protons with the paramagnetic electron localized at the octahedral site where a hydroxide group is co-ordinated originally: one of the two protons is the hydroxide proton. Another proton originates from a hydrogen-bonding  $[\text{NH}_3\text{Pr}^i]^+$  proton which is transferred to a bridging oxygen atom *trans* to the hydroxide group. Analysis of the e.s.r. parameters  $g$ ,  $^{95}\text{Mo}$  and  $^{97}\text{Mo}$  hyperfine, and  $^1\text{H}$  superhyperfine tensors has established that the maximum eigenvector of the  $^1\text{H}$  superhyperfine tensors with all positive signs lies close to the  $\text{Mo}^{\text{V}} \cdots \text{H}^+$  direction and that the superhyperfine couplings with the proton nuclei arise from a direct participation of the H  $1s$  orbital in the semioccupied molecular orbital. Plausible locations of the protons, which give equal spin density in two hydrogen  $1s$  orbitals, have been estimated by extended-Hückel calculations on a neutral fragment model  $[\text{NH}_3][\text{H}_2\text{Mo}^{\text{VO}}_3(\text{OH})-(\text{H}_2\text{O})_2]$ , for the molybdenum(v) site. The calculated semioccupied molecular orbital consists mainly of the extensively mixed  $4d$  orbitals, the oxygen and nitrogen  $2p$  orbitals, and the two hydrogen  $1s$  orbitals. The two protons at this site are situated symmetrically at a distance of *ca.* 1.9 Å from the paramagnetic molybdenum atom and 1.43 Å from the nearest oxygen atom. The geometry of the site corresponds to the saddle zone in the full potential energy surface, which can be regarded as a transition state for the solution photochemistry.

The electronic structure of reduced polyoxometalates is of current interest from the viewpoint of  $d$  electrons interacting with protons in the anion lattice.<sup>1-3</sup> E.s.r. spectroscopy has been applied to a study of the extent of delocalization of the paramagnetic electron in such compounds. E.s.r. spectra of u.v.-irradiated single crystals of alkylammonium polyoxomolybdates such as  $[\text{NH}_3\text{Pr}^i]_6[\text{Mo}_8\text{O}_{26}(\text{OH})_2]\cdot 2\text{H}_2\text{O}$ ,<sup>4</sup>  $[\text{NH}_3\text{-Pr}^i]_6[\text{Mo}_7\text{O}_{24}]\cdot 3\text{H}_2\text{O}$ ,<sup>5</sup>  $[\text{NH}_3\text{Pr}^i]_6[\text{Mo}_7\text{O}_{24}]\cdot 3\text{H}_2\text{O}$ ,<sup>6</sup> and  $[\text{NH}_3\text{Me}]_8[\text{Mo}_{10}\text{O}_{34}]\cdot 2\text{H}_2\text{O}$ <sup>7</sup> show that the unpaired electron is localized on a single  $\text{MoO}_6$  octahedral site in the anion lattice and interacts with the proton transferred from an alkylammonium nitrogen to a bridging oxygen atom.<sup>1</sup> On the other hand a perfect delocalization of the unpaired electron is found for the decatungstate  $[\text{W}_{10}\text{O}_{32}]^{5-}$  which has a dimeric structure of five edge-shared  $\text{WO}_6$  octahedra with approximately linear W-O-W bridges.<sup>2</sup> The e.s.r. spectrum of the single crystal of  $[\text{NH}_2\text{Pr}^i]_4[\text{H}_5\text{O}_2][\text{W}_{10}\text{O}_{32}]\cdot 6\text{H}_2\text{O}$  shows that the unpaired electron interacts with eight magnetically equivalent protons hydrogen-bonded to the terminal oxygen atoms at eight equatorial  $\text{WO}_6$  sites and that the semi-occupied molecular orbital (s.o.m.o.) consists of an orbital mixing among four sets of  $p_\pi-d_\pi-p_\pi-d_\pi-p_\pi$  O=W-O-W=O multiple bonds (W-O-W bond angle about  $180^\circ$ )<sup>8</sup> of the corner-shared equatorial  $\text{WO}_6$  octahedra. A large proton superhyperfine interaction of  $(5-12) \times 10^{-4} \text{ cm}^{-1}$  for the paramagnetic polyoxometalates of Mo and W suggests the direct participation of H  $1s$  orbitals in the s.o.m.o., which indicates that the maximum principal component of the  $^1\text{H}$ -superhyperfine tensors is approximately close to the proton paramagnetic electron direction.<sup>1,2</sup> In order to obtain details of the molecular orientation of the  $g$ , hyperfine and  $^1\text{H}$ -superhyperfine tensors

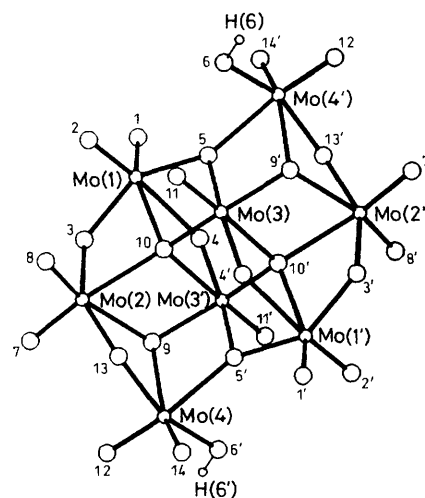


Figure 1. Structure of  $[\text{Mo}_8\text{O}_{26}(\text{OH})_2]^{6-}$  with the atom numbering scheme. Primed atoms are related to corresponding unprimed ones by an inversion centre

at the paramagnetic site, therefore, we decided to reinvestigate the e.s.r. spectrum of the u.v.-irradiated  $[\text{NH}_3\text{Pr}^i]_6[\text{Mo}_8\text{O}_{26}(\text{OH})_2]\cdot 2\text{H}_2\text{O}$ , in which the paramagnetic centre could be identified easily.<sup>4</sup> Figure 1 shows the structure of  $[\text{Mo}_8\text{O}_{26}(\text{OH})_2]^{6-}$  with the atom labelling. The two hydrogen atoms are attached to O(6) and O(6') at sites Mo(4') and Mo(4), respectively.<sup>9</sup> The photoreducible site is the Mo(4) or Mo(4') octahedral site which originally co-ordinates a hydroxide group. Figure 2 shows the environment<sup>9</sup> of the distorted Mo(4) site and the mode of solid-state photoreaction.<sup>1,6</sup> It has been proposed that the reduction of  $\text{Mo}^{\text{VI}}(4)$  to  $\text{Mo}^{\text{V}}(4)$  proceeds *via*

† Part 7 is ref. 7.

‡ Non-S.I. units employed:  $G = 10^{-4} \text{ T}$ ,  $\text{eV} \approx 1.60 \times 10^{-19} \text{ J}$ .

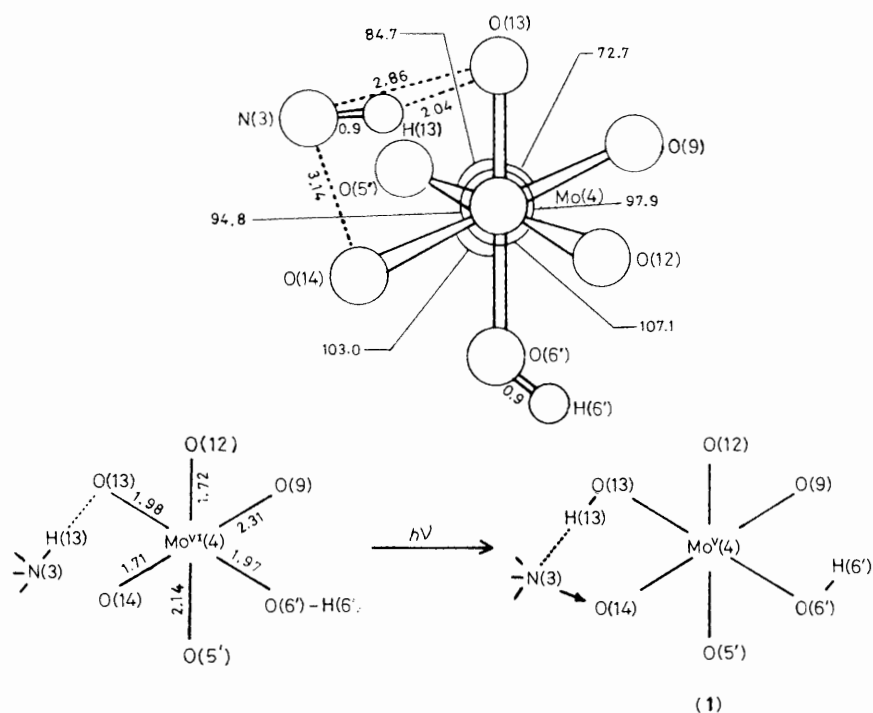


Figure 2. Bond distances (Å) and angles ( $^{\circ}$ ) in the environment of the Mo(4) site in the anion and the mode of the photoreaction

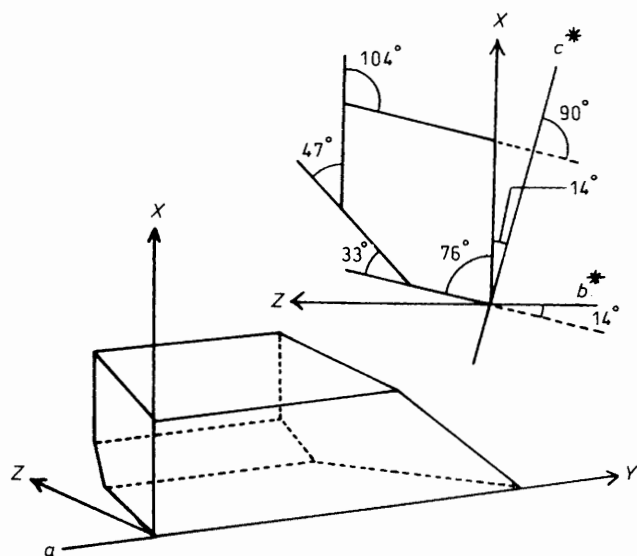


Figure 3. E.s.r. reference axes ( $X$ ,  $Y$ ,  $Z$ ) and crystallographic directions for an idealized crystal of  $[\text{NH}_3\text{Pr}^{\text{I}}]_6[\text{Mo}_8\text{O}_{26}(\text{OH})_2] \cdot 2\text{H}_2\text{O}$

photoexcitation of the oxygen-to-molybdenum charge-transfer band of a terminal Mo(4)–O(14) bond with an accompanying transfer of hydrogen H(13) from  $[\text{NH}_3\text{Pr}^{\text{I}}]^+ \text{N}(3)$  to bridging O(13), followed by an interaction of the non-bonding electrons of the resulting amino N(3) with terminal O(14) leading to a charge-transfer complex (1).<sup>4,6,7</sup> In this paper, furthermore, the location of the protons at the Mo<sup>V</sup>(4) site is discussed with the help of extended-Hückel calculations on a neutral fragment model for the Mo<sup>V</sup>(4) site.

### Experimental

Hexakis(isopropylammonium) dihydroxo-octamolybdate dihydrate  $[\text{NH}_3\text{Pr}^{\text{I}}]_6[\text{Mo}_8\text{O}_{26}(\text{OH})_2] \cdot 2\text{H}_2\text{O}$  was prepared using

a published method.<sup>10</sup> Single crystals were grown from a saturated aqueous solution (10 cm<sup>3</sup>) containing hexakis(isopropylammonium) heptamolybdate trihydrate  $[\text{NH}_3\text{Pr}^{\text{I}}]_6[\text{Mo}_7\text{O}_{24}] \cdot 3\text{H}_2\text{O}$  (5 g) at room temperature in the dark for 10 d. The crystal belongs to the space group  $P\bar{1}$ , the half molecule being related by a centre of inversion:  $a = 10.66(1)$ ,  $b = 12.19(1)$ ,  $c = 9.65(2)$  Å,  $\alpha = 104.6(2)$ ,  $\beta = 82.1(5)$ , and  $\gamma = 96.5(2)^{\circ}$ , and  $Z = 1$ .<sup>9</sup> An orthogonal axis system was chosen in the crystal: the  $Y$  axis coincident with the  $a$  axis direction, the  $Z$  axis coincident with the  $b^*$  axis, and the  $X$  axis perpendicular to  $Y$  and  $Z$ . Figure 3 shows the axis system and crystal morphology. The orientation of the body-fixed orthogonal axes with respect to the crystallographic axes was determined by both oscillation and Weissenberg photographs. A single crystal about 1.8 mm long and 0.7–1.0 mm thick was irradiated at room temperature with u.v. light of  $\lambda \geq 313$  nm. After 1 h it was reddish brown. E.s.r. experiments were performed on a Varian E-12  $X$ -band spectrometer at room temperature, using diphenylpicrylhydrazyl as a field marker. Spectra were recorded in the three orthogonal planes  $XY$ ,  $YZ$ , and  $ZX$ , the crystal being fixed by use of silicon grease on a vertical quartz rod able to rotate the magnet around its axis. Diffuse reflectance spectra (380–1500 nm) were recorded for  $[\text{NH}_3\text{Pr}^{\text{I}}]_6[\text{Mo}_8\text{O}_{26}(\text{OH})_2] \cdot 2\text{H}_2\text{O}$  powder at room temperature with a Hitachi 330 spectrophotometer. The atomic orbitals used for the extended-Hückel calculations were simple Slater-type orbitals except for molybdenum  $4d$  orbitals where a linear combination of two Slater functions was chosen.<sup>11</sup> The parameters for all atoms used are listed in Table 1. The Wolfsberg–Helmholtz proportionality constant  $K$  was set at 1.75.

### Results

The e.s.r. spectrum of the u.v.-irradiated single crystal of  $[\text{NH}_3\text{Pr}^{\text{I}}]_6[\text{Mo}_8\text{O}_{26}(\text{OH})_2] \cdot 2\text{H}_2\text{O}$  is shown in Figure 4(a) together with a diffuse reflectance spectrum of the u.v.-irradiated powder of this compound. The two sets of lines reveal

**Table 1.** Parameters used in the extended-Hückel calculations

Orbital	$H_{ij}/\text{eV}$	$\zeta_1$
Mo* 4d	-12.30	4.54
5s	-9.66	1.956
5p	-6.36	1.90
O 2s	-32.3	2.275
2p	-14.8	2.275
N 2s	-26.0	1.95
2p	-13.4	1.95
C 2s	-21.4	1.625
2p	-11.4	1.625
H 1s	-13.6	1.3

\* Coefficients used in the double- $\zeta$  expansion ( $\zeta_2 = 1.90$ ) of the  $d$  orbitals were  $C_1 = C_2 = 0.5899$ .

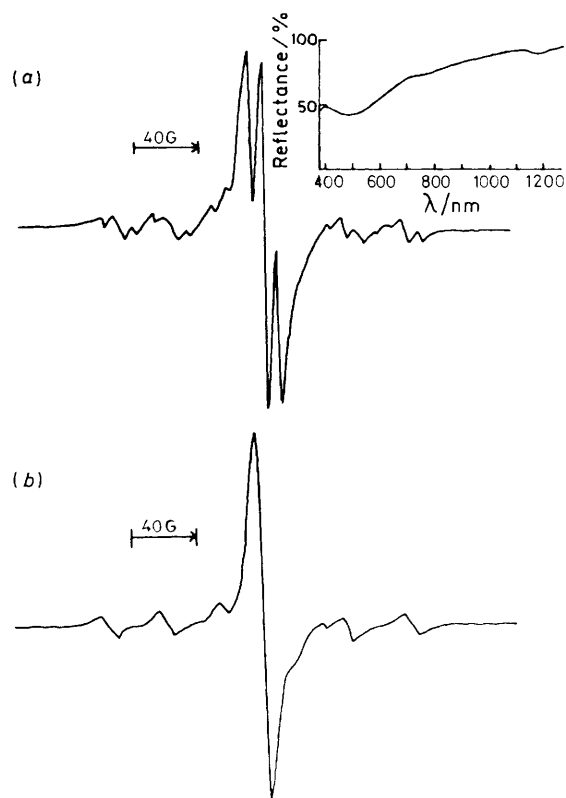


**Figure 4.** Examples of the e.s.r. spectra obtained with u.v.-irradiated crystals of  $[\text{NH}_3\text{Pr}]_6[\text{Mo}_8\text{O}_{26}(\text{OH})_2]\cdot 2\text{H}_2\text{O}$  (a) and the deuteriated compound (b).  $H_0$  is in the  $ZX$  plane along the  $Z$  axis. Insert: diffuse reflectance spectrum of the u.v.-irradiated sample

the presence of a localized paramagnetic site,  $\text{Mo}^{\text{V}}\text{O}_4(\text{OH})_2$  which exhibits a 1:2:1 triplet and a sextet of triplets. The first set is attributed to the interaction (ca. 10 G) of the unpaired electron with two  $^1\text{H}$  nuclei ( $I = \frac{1}{2}$ ). The nature of this more intense set of lines corresponds to the  $^{96}\text{Mo}$  atom ( $I = 0$ ). The second set of lines, of lower intensity, characterizes the hyperfine spectrum of  $^{95}\text{Mo}$  and  $^{97}\text{Mo}$  further split by the same superhyperfine interaction of the first set of lines. The relative intensity of the two sets of lines is in good agreement with the molybdenum isotopic composition. The two molybdenum isotopes,  $^{95,97}\text{Mo}$ , in total natural abundance (25.25%) have the same nuclear spin ( $I = \frac{5}{2}$ ) and nearly the same magnetic moment, so that it is not possible to resolve the separate

**Table 2.** E.s.r. parameters for the  $\text{Mo}^{\text{V}}(4)$  centre<sup>a</sup>

Principal values <sup>b</sup>	Direction cosines with respect to		
	X	Y	Z
$g_1$ 1.958	-0.5562	0.7201	-0.4147
$g_2$ 1.935	-0.3283	0.2680	0.9057
$g_3$ 1.901	0.7634	0.6400	0.0874
$g_0$ 1.931			
$A_{\text{Mo}1}$ 76.8	0.2796	0.9108	0.3036
$A_{\text{Mo}2}$ 35.9	-0.7373	0.0011	0.6756
$A_{\text{Mo}3}$ 19.4	0.6150	-0.4127	0.6719
$A_{\text{Mo}0}$ 44.0			
$A_{\text{H}1}$ 8.94	0.9902	0.0432	0.1325
$A_{\text{H}2}$ 8.41	-0.1389	0.2263	0.9641
$A_{\text{H}3}$ 6.78	0.0117	-0.9731	0.2301
$A_{\text{H}0}$ 8.05			

<sup>a</sup>  $g$  and  $A_{\text{H}i}$  values for  $[\text{Mo}_8\text{O}_{26}(\text{OH})_2]^{6-}$  in previous papers<sup>1,4</sup> should be corrected to the present values due to the high signal/noise ratio corresponding to the latter. <sup>b</sup>  $g_0 = (g_1 + g_2 + g_3)/3$ ; units of  $A$  are  $10^{-4} \text{ cm}^{-1}$ ,  $A_{\text{Mo}0} = (A_{\text{Mo}1} + A_{\text{Mo}2} + A_{\text{Mo}3})/3$  and  $A_{\text{H}0} = (A_{\text{H}1} + A_{\text{H}2} + A_{\text{H}3})/3$ .

hyperfine lines. The line separation of the 1:2:1 triplet was observed at all orientations of the magnetic field, resulting from the magnetic equivalence of the two H atoms at the paramagnetic site. Thus, we can reconfirm that the paramagnetic electron is localized at either the  $\text{Mo}(4)$  or  $\text{Mo}(4')$  octahedral site where a hydroxide group of  $\text{O}(6')\text{-H}(6')$  or  $\text{O}(6)\text{-H}(6)$  is coordinated originally and that another H atom at the paramagnetic  $\text{Mo}^{\text{V}}\text{O}_4(\text{OH})_2$  site is a hydrogen-bonding  $\text{H}(13)$  [or  $\text{H}(13')$ ] bound to  $\text{O}(13)$  [or  $\text{O}(13')$ ] *trans* to  $\text{O}(6')$  [or  $\text{O}(6)$ ],<sup>4</sup> as shown in Figure 2. Similar treatment of a deuteriated sample,  $[\text{ND}_3\text{Pr}]_6[\text{Mo}_8\text{O}_{26}(\text{OD})_2]\cdot 2\text{D}_2\text{O}$  prepared in  $\text{D}_2\text{O}$ , resulted in collapse of the triplets in the e.s.r. spectrum, as shown in Figure 4(b). Figure 4(b) shows that the peak-to-peak linewidth of 6–7 G is too broad for  $^2\text{H}$  superhyperfine interaction to be resolved, since the resonance frequency for  $^2\text{H}$  is  $1/6.5$  compared with that for  $^1\text{H}$ .

The spectrum has been interpreted using the spin Hamiltonian in equation (1) with  $S = \frac{1}{2}$ ,  $I_{\text{Mo}} = \frac{5}{2}$ , and  $I_{\text{H}} = \frac{1}{2}$ .

$$\mathcal{H} = \beta H \cdot g \cdot S + I_{\text{Mo}} \cdot A_{\text{Mo}} \cdot S + \sum_{\text{H}} I_{\text{H}} \cdot A_{\text{H}} S \quad (1)$$

Figure 5 shows the angular variation of the e.s.r. spectrum of the paramagnetic centre for the rotation of the magnetic field in the planes  $XY$ ,  $YZ$ , and  $ZX$ . The e.s.r. tensors  $g$ ,  $A_{\text{Mo}}$ , and  $A_{\text{H}}$  have been obtained using successively a least-squares fitting subroutine and direct diagonalization of the Hamiltonian. The results are given in Table 2. The choice of sign for the tensor components of the site is the same as for  $[\text{Mo}_7\text{O}_{24}]^{6-}$ .<sup>6</sup> A plot of the angular dependence of the  $g$  values for the site in the crystal  $XY$  plane reaches a maximum (1.953) at ca.  $30^\circ$  from the  $Y$  axis. This value almost approaches the highest of the principal  $g$  values,  $g_1(1.958)$ ; hence these directions in the  $XY$  plane approach that of the vector  $g_1$ . In the  $XY$  plane, furthermore, at ca.  $40^\circ$  from the  $X$  axis, the minimum value (ca. 1.898) is obtained. This value approaches  $g_3 = 1.901$ ; hence its direction could be considered nearly coincident with that of  $g_3$ . Similarly, a plot of the angular dependence of  $A_{\text{Mo}}$  in the crystal  $XY$  plane has its maximum ( $75.3 \times 10^{-4} \text{ cm}^{-1}$ ) at ca.  $30^\circ$  from the  $Y$  axis. This direction approaches that of  $A_{\text{Mo}1}$ . Plots of the angular dependence of  $A_{\text{H}}$  have maxima at  $9.37 \times 10^{-4}$  (ca.  $10^\circ$  from the  $X$  axis) and  $9.12 \times 10^{-4} \text{ cm}^{-1}$  (ca.  $10^\circ$  from the  $X$  axis) in the  $XY$  and  $XZ$  planes, respectively. These directions approach that of

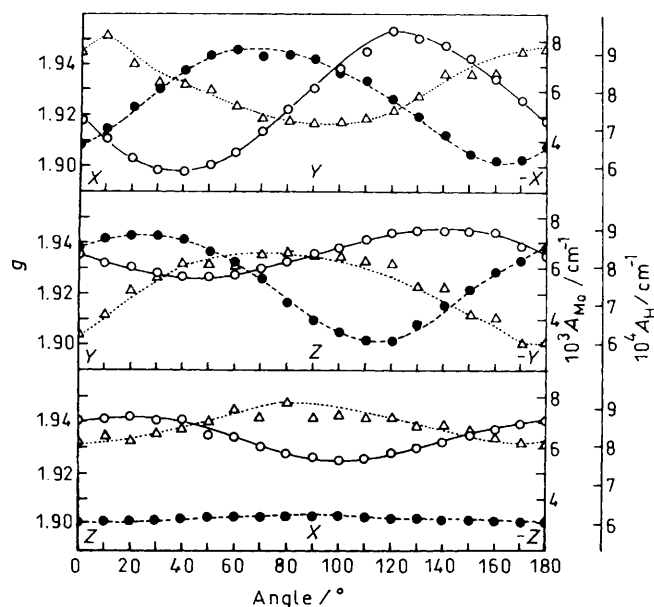


Figure 5. Angular dependence of the signals in the  $XY$ ,  $YZ$ , and  $ZX$  planes:  $g$  (○),  $A_{Mo}$  (●), and  $A_H$  (△)

Table 3. Angles (°) between the  $g$ ,  $A_{Mo}$ , and  $A_H$  tensors for the molybdenum centre\*

	$A_{Mo1}$	$A_{Mo2}$	$A_{Mo3}$	$A_{H1}$	$A_{H2}$	$A_{H3}$
$g_1$	68	83	23	122	81	37
$g_2$	65	31	107	101	168	87
$g_3$	35	120	105	37	97	54
$A_{Mo1}$				69	117	36
$A_{Mo2}$				130	139	98
$A_{Mo3}$				133	62	56

\* Reliable to  $\pm 1^\circ$ .

Table 4. Angles (°) between the molecular  $g$ ,  $A_{Mo}$ , and  $A_H$  values and the chosen molecular directions at the Mo(4) site\*

	Alternative 1								
	$g_1$	$g_2$	$g_3$	$A_{Mo1}$	$A_{Mo2}$	$A_{Mo3}$	$A_{H1}$	$A_{H2}$	$A_{H3}$
Mo(4)–O(5')	105	53	41	38	84	128	51	136	74
Mo(4)–O(6')	74	27	111	79	12	85	128	142	86
Mo(4)–O(9)	43	83	48	29	98	63	85	95	7
Mo(4)–O(12)	128	61	51	60	89	150	41	130	95
Mo(4)–O(13)	97	138	48	79	169	94	43	52	75
Mo(4)–O(14)	23	85	68	46	90	44	104	89	14
Mo(4)···N(3)	42	67	118	86	48	43	155	101	68
Mo(4)···H(6')	62	47	124	89	22	68	148	122	85
Mo(4)···H(13)	44	59	116	82	41	51	150	110	69
	Alternative 2								
Mo(4)–O(5')	23	111	100	87	96	7	126	59	52
Mo(4)–O(6')	89	141	51	79	168	85	51	47	69
Mo(4)–O(9)	46	66	54	23	82	69	90	111	21
Mo(4)–O(12)	42	116	121	109	91	19	138	53	74
Mo(4)–O(13)	71	36	119	86	11	79	137	133	89
Mo(4)–O(14)	65	66	36	3	90	87	71	116	33
Mo(4)···N(3)	105	101	18	53	132	115	21	88	70
Mo(4)···H(6')	103	127	40	73	158	104	31	63	76
Mo(4)···H(13)	100	108	21	55	139	108	26	81	66

\* Error  $\pm 2^\circ$ .

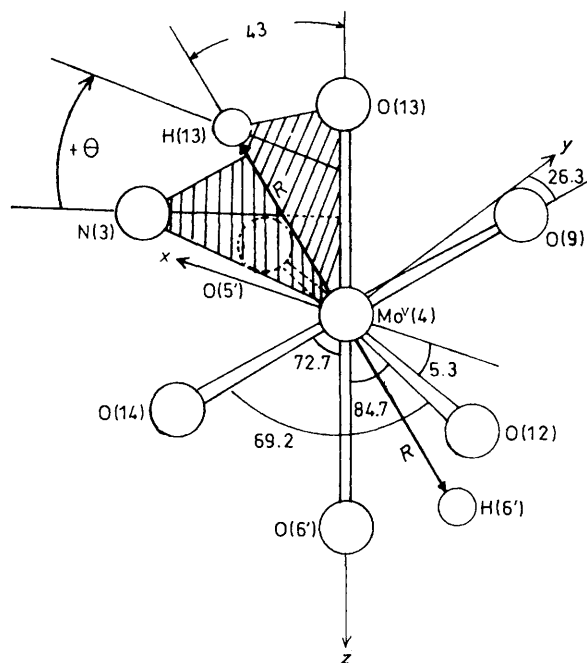
the vector  $A_{H1}$ . The plots show minima at  $7.10 \times 10^{-4}$  and  $6.00 \times 10^{-4} \text{ cm}^{-1}$  at *ca.* 0 and  $170^\circ$  from the  $Y$  axis in the  $XY$  and  $YZ$  planes, respectively. The values are close to that of  $A_{H3} = 6.78 \times 10^{-4} \text{ cm}^{-1}$  and the directions approach that of the vector  $A_{H3}$ . Table 2 shows the direction cosines of the tensors which give the best fit based on the above considerations.

Table 3 shows the angles between the  $g$ ,  $A_{Mo}$ , and  $A_H$  eigenvectors. The non-coincidence of the principal axes of the tensors  $g$  and  $A$  suggests the displacement of the directions of the principal  $g$  values from the Mo–O axis, due to a  $d$ -orbital mixing. Table 4 shows the angles between the Mo–O molecular axes for the Mo(4) site and the eigenvectors  $g$ ,  $A_{Mo}$ , and  $A_H$ . The two alternative sets of angles are attributed to two sets of orientations of the crystallographic axes ( $a$ ,  $b$ ,  $c$ ) with respect to the body-fixed orthogonal axes ( $X$ ,  $Y$ ,  $Z$ ) as shown in Figure 3. The observable displacement of the  $g$  tensors from the Mo–O axes for the Mo(4) site provides evidence in support of the  $d$ -orbital mixing arising from the low-symmetry ligand field, if there is no significant configuration change in the Mo–O axes at the Mo(4) site upon u.v. irradiation. The vector  $A_{Mo2}$  makes an angle of  $169^\circ$  in alternative 1 ( $11^\circ$  in alternative 2) with the Mo(4)–O(13) bond axis and  $A_{H3}$  subtends an angle of  $14^\circ$  in the alternative 1 ( $33^\circ$  in alternative 2) with Mo(4)–O(14). Thus, it is possible to say that the eigenvectors  $A_{Mo2}$  and  $A_{H3}$  are close to the Mo–O molecular axes involving oxygen atoms associated with the interaction with the transferable proton and amino nitrogen in the charge-transfer complex (Figure 2). Furthermore, vector  $A_{H1}$  in alternative 1 is inclined at  $150^\circ$  to Mo(4)···H(13) and at  $148^\circ$  to Mo(4)···H(6') ( $26$  and  $31^\circ$  in alternative 2). Since H(13) will be transferred from N(3) to O(13) at the paramagnetic Mo<sup>V</sup>(4) site (Figure 2),  $A_{H1}$  will be closer to a resultant Mo<sup>V</sup>(4)···H(13) direction. This seems to allow the maximum component of the  $A_H$  tensors to define the Mo<sup>V</sup>···H<sup>+</sup> direction involving the proton transferred from the alkylammonium nitrogen to the bridging oxygen in the polyoxomolybdates, as suggested by the analysis of the e.s.r. parameters based on the point-dipole approximation which indicated a direct participation of the H 1s orbital in the s.o.m.o.<sup>2,6,7</sup> Then, the signs of the components of the  $A_H$  tensors are positive.

**Table 5.** Spin density in the dominant atomic orbitals for the six positions of H(13) chosen

Conformation	(2.5, -10)	(2.1, -5)	(1.9, -10)	(1.8, -10)	(1.7, -10)	(1.1, -20)
Mo(4) 5s	0.008	0.017	0.015	0.014	0.012	0.001
4d <sub>z<sup>2</sup></sub>	0.019	0.037	0.038	0.037	0.035	0.028
4d <sub>x<sup>2</sup>-y<sup>2</sup></sub>	0.037	0.083	0.079	0.076	0.072	0.053
4d <sub>xy</sub>	0.018	0.028	0.030	0.029	0.027	0.027
4d <sub>yz</sub>	0.085	0.306	0.310	0.305	0.300	0.302
O(6') 2p <sub>x</sub>	0.008					
2p <sub>y</sub>	0.269	0.201	0.181	0.178	0.214	0.195
2p <sub>z</sub>						0.045
O(12) 2p <sub>y</sub>	0.017	0.023	0.025	0.026	0.028	0.031
O(13) 2p <sub>y</sub>		0.029	0.049	0.056	0.062	0.086
O(14) 2p <sub>z</sub>		0.032	0.043	0.049	0.055	0.179
N(3) 2p <sub>y</sub>		0.020	0.023	0.021	0.018	
2p <sub>z</sub>		0.013	0.015	0.014	0.012	
H(6') 1s	0.517	0.139	0.091	0.080	0.110	0.067
H(13) 1s	0.001	0.029	0.057	0.067	0.076	0.121
ΣS <sup>a</sup>	0.981	0.956	0.954	0.952	1.020	1.109
E(R, θ) <sup>b</sup>	0.4	1.3	1.2	1.0	0.8	0

<sup>a</sup> ΣS = Total spin density of the atomic orbitals chosen. <sup>b</sup> E(R, θ) = Total bonding energy (eV mol<sup>-1</sup>) of the chosen conformation relative to the conformation (1.1, -20).



**Figure 6.** Neutral fragment  $[\text{NH}_3][\text{H}_2\text{Mo}^{\text{V}}\text{O}_3(\text{OH})(\text{H}_2\text{O})_2]$  used for extended-Hückel calculations of the  $\text{Mo}^{\text{V}}(4)$  site and  $R$  and  $\theta$  definitions. Angles in  $^\circ$ . Positions of H atoms except  $\text{H}(6')$  and  $\text{H}(13)$  are omitted for clarity

To obtain a description of the location of the protons at the  $\text{Mo}^{\text{V}}(4)$  site, calculations were carried out for a neutral fragment model (Figure 6): boundary bridging oxygen atoms are saturated by hydrogen atoms which replace the neighbouring Mo atoms. The resultant bond distance between the hydrogen and

oxygen atom is taken to be equal to  $(\text{Mo}-\text{O}$  bond length/1.97)  $\times$  (O-H bond distance of water, 0.96 Å<sup>12</sup>) where 1.97 Å is the average of the  $\text{Mo}(4)-\text{O}(13)$  and  $\text{Mo}(4)-\text{O}(6')$  bond lengths. To simplify the extended-Hückel calculation, the following assumptions were made: (i) the isopropyl substituent of  $[\text{NH}_3\text{Pr}^{\text{I}}]^+$  was replaced by an H atom 1.0 Å<sup>12</sup> distant from N(3); (ii)  $\text{NH}_3$  in the resultant  $[\text{NH}_3\text{H}(13)]^+$ ,  $\text{Mo}(4)$ , and the three bridging oxygen atoms O(5'), O(9), and O(13) hardly change their positions during u.v. irradiation; accordingly, the positions of these atoms are available from the X-ray crystal structure<sup>10</sup> of  $[\text{Mo}_8\text{O}_{26}(\text{OH})_2]^{6-}$ ; (iii) each configuration of O(13)- $\text{Mo}(4)$ -O(6'), O(5')- $\text{Mo}(4)$ -O(12), and O(9)- $\text{Mo}(4)$ -O(14) is linear; (iv) the bond distances  $\text{Mo}(4)-\text{O}(6')$  and  $\text{Mo}(4)=\text{O}(12)$  hardly change upon u.v. irradiation, but  $\text{Mo}(4)-\text{O}(14)$  is altered to a single bond of 1.97 Å, due to the charge-transfer complex formation (Figure 2); (v) H(13) and H(6'), which will be located around O(13) and O(6') respectively, are related by an inversion centre at the  $\text{Mo}^{\text{V}}(4)$  atom due to their magnetic equivalence [Figure 4(a)]. Using the above assumptions it is, in principle, possible to determine the most plausible location of H(13) [and H(6')] at the  $\text{Mo}^{\text{V}}(4)$  site, allowing for the mixing of the Mo 4d wavefunctions and for Mo-O orbital mixing in the s.o.m.o. The O(13)- $\text{Mo}^{\text{V}}(4)$ -O(6') molecular axis was chosen as the z axis and the  $\text{Mo}^{\text{V}}(4)$ -O(5') bond axis viewed in projection along z axis as the x axis. The parameters  $R$  and  $\theta$  were generally used to estimate the location of H(13) at the  $\text{Mo}^{\text{V}}(4)$  site:  $R$  is the  $\text{Mo}^{\text{V}}(4) \cdots \text{H}(13)$  distance (Å) and  $\theta$  is the dihedral angle ( $^\circ$ ) between the two planes N(3)Mo(4)O(13) and H(13)Mo(4)O(13) as shown in Figure 6. The angle H(13)- $\text{Mo}^{\text{V}}(4)$ -O(13) was kept at 43° which is the angle between the vector  $A_{\text{H}1}$  and the Mo(4)-O(13) molecular axis (Table 4).

To characterize the shape of the full potential-energy surface  $E(R, \theta)$  for each conformation given by its  $R$  and  $\theta$  values in polar co-ordinates, the total bonding energy for the 57 valence electrons was calculated by taking into account the occupation number of each molecular orbital and the sum over all

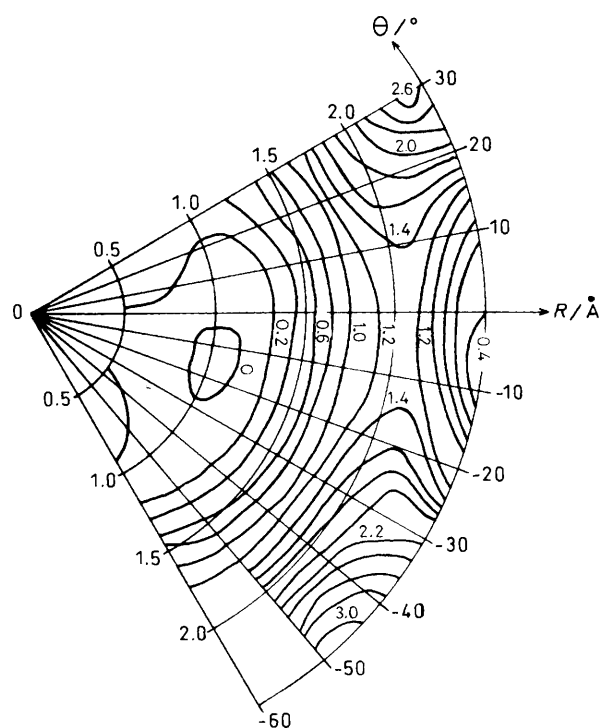


**Figure 7.** Total bonding-energy surface  $E(R, \theta)$  for the neutral fragment model of the  $\text{Mo}^{\text{V}}(4)$  site. Numbers indicate the relative energies (eV) of  $E(R, \theta)$  at various  $R$  and  $\theta$  in polar co-ordinates, contoured at intervals of 0.2 eV

molecular orbitals. Figure 7 shows the relative energies  $E(R, \theta)$  on variation of  $R$  and  $\theta$ . We also calculated the spin density in atomic orbital  $i$ ,  $\sum_j C_i C_j S_{ij}$  where  $C_i$  (or  $C_j$ ) and  $S_{ij}$  are the atomic orbital coefficient and overlap integral between atomic orbitals  $i$  and  $j$ , respectively. Table 5 shows the calculated spin density in each of the dominant atomic orbitals for six conformations  $(R, \theta) = (2.5, -10), (2.1, -5), (1.9, -10), (1.8, -10), (1.7, -10)$ , and  $(1.1, -20)$ . The most plausible conformation of the  $\text{Mo}^{\text{V}}(4)$  site, which would give approximately equal spin density in the H(13) and H(6') 1s orbitals, is  $(1.9, -10)$  as discussed below.

### Discussion

The point-dipole approximation is used in analysing  $A_{\text{Mo}}$  and  $A_{\text{H}}$  tensors. Under the approximation that the hyperfine tensors are axial with  $A_{\text{Mo}\parallel} = 76.8 \times 10^{-4} \text{ cm}^{-1}$  and  $A_{\text{Mo}\perp} = (19.4 + 35.9)/2 \times 10^{-4} = 27.6 \times 10^{-4} \text{ cm}^{-1}$ , defining an anisotropic hyperfine parameter for  $d$  orbitals as  $7(A_{\text{Mo}\parallel} - A_{\text{Mo}\perp})/6$  and dividing its value,  $57.3 \times 10^{-4} \text{ cm}^{-1}$ , by the anisotropic hyperfine parameter  $P = g\beta\gamma_{\text{Mo}} \langle r^{-3} \rangle_{4d}$  for  $^{95,97}\text{Mo}$  ( $150.7 \text{ MHz}^{13} = 50.3 \times 10^{-4} \text{ cm}^{-1}$ ), gives an estimate of 1.128 for the spin population in the Mo 4d orbitals, when  $A_{\text{Mo}\parallel}$  and  $A_{\text{Mo}\perp}$  have the same sign. If  $A_{\text{Mo}\parallel}$  and  $A_{\text{Mo}\perp}$  are assumed to have opposite signs an estimated Mo 4d contribution of 2.078 is obtained. This constitutes an unacceptably large total spin density and strongly implies that the  $A_{\text{Mo}}$  tensors have the same sign. The derived isotropic component  $A_{\text{Mo}0} (= 44.0 \times 10^{-4} \text{ cm}^{-1})$  is quite similar to that  $[(45-46) \times 10^{-4} \text{ cm}^{-1}]$  observed for the paramagnetic species having  $\langle g \rangle = 1.921$  in the solution photolyte.<sup>5,6</sup> The isotropic hyperfine interaction for unit spin density in a Mo 5s orbital, which is obtained by computing the isotropic hyperfine interaction  $A = (8\pi g\beta\gamma/3)\psi^2(0)$ , is  $66.2 \times$

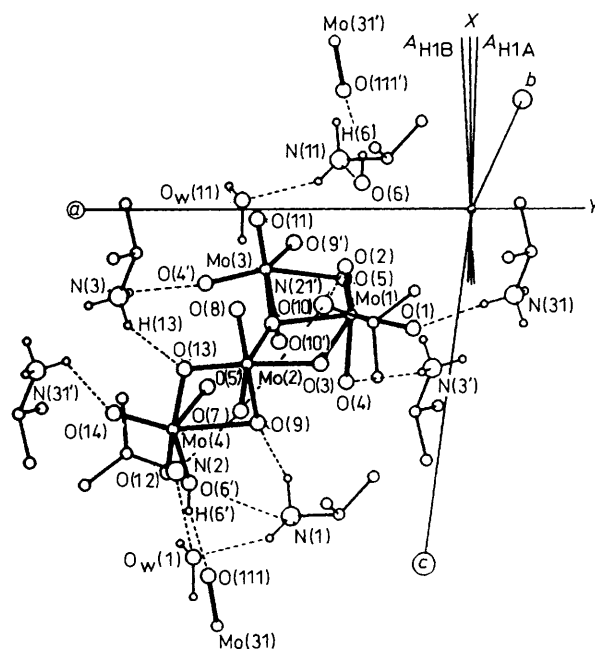


**Figure 8.** Molecular structure of a half moiety of  $[\text{NH}_3\text{Pr}]_6[\text{Mo}_8\text{O}_{26}(\text{OH})_2] \cdot 2\text{H}_2\text{O}$ , viewed in projection along the  $Z$  axis.  $A_{\text{H1A}}$  and  $A_{\text{H1B}}$  denote the principal  $A_{\text{H}}$  directions in alternatives 1 and 2, respectively. Atoms Mo(31), O(111), N(11), N(21), N(31), and  $\text{O}_w(11)$  denote Mo(3), O(11), N(1), N(2), N(3), and water oxygen  $\text{O}_w(1)$  atoms in the adjacent unit cell

$10^{-4} \text{ cm}^{-1}$ , where  $\psi^2(0)$  is the atomic parameter;<sup>13</sup> hence a Mo 5s contribution of 0.059 is indicated. Reasonable agreement with both the sign and magnitude of the  $A_{\text{H}}$  tensors is obtained only by using all positive signs (Table 2), as discussed for  $[\text{NH}_3\text{Pr}]_6[\text{Mo}_7\text{O}_{24}] \cdot 3\text{H}_2\text{O}^6$  and  $[\text{NH}_3\text{Me}]_8[\text{Mo}_8\text{O}_{26}(\text{MoO}_4)_2] \cdot 2\text{H}_2\text{O}^7$ . This leads to the idea that the maximum principal value of the  $^1\text{H}$  superhyperfine tensor lies close to the  $\text{Mo}^{\text{V}} \cdots \text{H}$  direction, which was available for the determination of the paramagnetic site in the polyoxomolybdate lattice.<sup>1</sup> Then, the tensors can be separated as shown below.

$$\begin{pmatrix} +8.94 \\ +8.41 \\ +6.78 \end{pmatrix} \times 10^{-4} \text{ cm}^{-1} = \left[ 8.05 + \begin{pmatrix} +0.89 \\ +0.86 \\ -1.27 \end{pmatrix} \right] \times 10^{-4} \text{ cm}^{-1}$$

A value of 0.017 ( $= 8.05 \times 10^{-4} \text{ cm}^{-1}/474 \times 10^{-4} \text{ cm}^{-113}$ ) can be estimated for the spin population in a H 1s orbital, which leads to a value of 0.034 ( $= 2 \times 0.017$ ) for the two H 1s contributions to the s.o.m.o. The total spin density for the  $\text{Mo}^{\text{V}}(4)$  site is therefore  $1.128 + 0.059 + 0.034 = 1.221$ , which is close to unity. If H(13) [or H(6')] lies in the nodal plane of the s.o.m.o. and the spin density on  $\text{Mo}^{\text{V}}(4)$  does not contribute to the spin polarization of the O(13)-H(13) [or O(6')-H(6')] bond, the isotropic coupling constant provides the negative spin density at H(13) [or H(6')] and is simply related to the spin density on O(13) [or O(6')]. By using the known parameters of the  $\alpha$  proton in the  $\dot{\text{C}}\text{H}$   $\pi$ -radical system,<sup>14</sup> then the spin-density distribution on O(13) [or O(6')] can be estimated. In calculations for  $(A_{\text{H1}}, A_{\text{H2}}, A_{\text{H3}}) = (-8.94 \times 10^{-4} \text{ cm}^{-1}, -8.41 \times 10^{-4} \text{ cm}^{-1}, -6.78 \times 10^{-4} \text{ cm}^{-1})$ , the OH bond is 40% ionic<sup>15</sup> so that the spin density on O(13) [or O(6')] is taken to be  $A_{\text{iso}} (= 8.05 \times 10^{-4} \text{ cm}^{-1}/12.0 \times 10^{-4} \text{ cm}^{-1}) = 0.67$ . This value is unreasonably large, considering  $0.67 \times 2 = 1.3$  as the total spin density of O(13) and O(6'). Any other choice of  $A_{\text{H}}$  sign results in a physically improbable hyperfine interaction

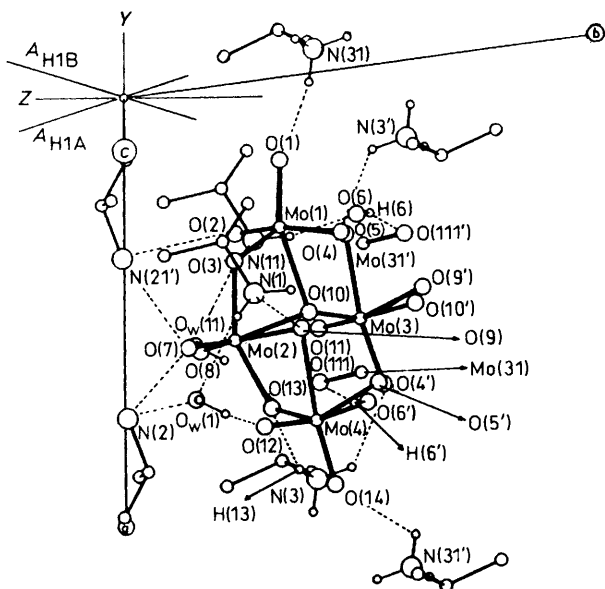


**Figure 9.** Molecular structure of a half moiety of  $[\text{NH}_3\text{Pr}]_6[\text{Mo}_8\text{O}_{26}(\text{OH})_2]\cdot 2\text{H}_2\text{O}$ , viewed in the projection along the  $X$  axis. Notations as in Figure 8

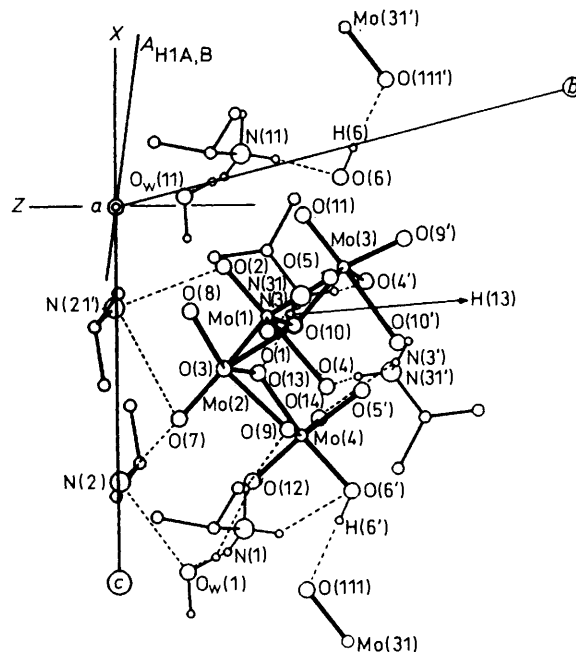


**Figure 10.** Molecular structure of a half moiety of  $[\text{NH}_3\text{Pr}]_6[\text{Mo}_8\text{O}_{26}(\text{OH})_2]\cdot 2\text{H}_2\text{O}$ , viewed in the projection along the  $Y$  axis. Notations as in Figure 8

with the  $\alpha$  proton of  $\dot{\text{O}}\text{H}$  fragment.\* Therefore, it is expected that a twist about the  $\text{Mo}^{\text{V}}(4)\text{--O}(13)$  [or  $\text{Mo}^{\text{V}}(4)\text{--O}(6')$ ] bond occurs and that  $\text{O}(13)\text{--H}(13)$  [or  $\text{O}(6')\text{--H}(6')$ ] no longer lies in the nodal plane of the s.o.m.o., resulting in a direct spin polarization which produces a positive spin density at the H atoms analogous to that of the  $\beta$  protons of a  $\dot{\text{C}}\text{OH}$  system. In contrast to the high anisotropy of the  $\alpha$ -proton interaction, the interactions of  $\beta$  protons are almost isotropic and the principal values of the anisotropic tensor rarely exceed 10% of the isotropic hyperfine interaction.<sup>14</sup> Thus,  $A_{\text{H}}$  tensors with all positive signs are proposed (Table 2) and both H(13) and H(6') are expected to occupy positions such that  $\text{Mo}^{\text{V}}\cdots\text{H}$  is approximately in the direction of the largest component of the  $A_{\text{H}}$  tensors.<sup>16</sup>

The results in Table 4 imply that  $A_{\text{H}1} = 8.94 \times 10^{-4} \text{ cm}^{-1}$  is approximately close to the  $\text{Mo}^{\text{V}}(4)\cdots\text{H}(13)$  direction where H(13) is expected to be located in the range between  $1/3$  (ca. 1 Å) and  $2/3$  (ca. 2 Å) of the  $\text{N}(3)\cdots\text{O}(13)$  distance (2.86 Å) from O(13). The half molecules of  $[\text{NH}_3\text{Pr}]_6[\text{Mo}_8\text{O}_{26}(\text{OH})_2]\cdot 2\text{H}_2\text{O}$  viewed in projection along the  $X$ ,  $Y$ , and  $Z$  axes together with the projected  $A_{\text{H}1}$  direction are shown in Figures 8–10 where dotted lines indicate the hydrogen-bonding distances such as  $\text{N}(3)\text{--H}(13)\cdots\text{O}(13)$  and  $\text{O}(6')\text{--H}(6')\cdots\text{O}(111)$  in the dark. Figures 8–10 reveal that the  $\text{Mo}^{\text{V}}(4)\cdots\text{H}(13)$  direction resulting from the u.v.-induced transfer of H(13) from N(3) to O(13) is approximately in accord with the  $A_{\text{H}1}$  vector. The  $A_{\text{H}1}$  vector in alternative 1 is closer to  $\text{Mo}^{\text{V}}(4)\cdots\text{H}(13)$  than in alternative 2. Assuming that alternative 1 is correct, we can confirm the direct participation of H(13) and H(6') 1s orbitals in the s.o.m.o. and assign positive signs to the  $A_{\text{H}}$  tensors. In conjunction with the magnetic equivalence of H(13) and H(6') at the  $\text{Mo}^{\text{V}}(4)$  site [Figure 4(a)], the displacement ( $148^\circ$  in alternative 1) of the  $\text{Mo}(4)\cdots\text{H}(6')$  direction from the  $A_{\text{H}1}$  vector, therefore, implies that the injection of the paramagnetic

electron into the  $\text{Mo}(4)$  atom induces a change in configuration of  $\text{Mo}(4)\text{--O}(6')\text{--H}(6')$ . This let us assume symmetric linear geometries for  $\text{H}(13)\cdots\text{Mo}^{\text{V}}(4)\cdots\text{H}(6')$  and  $\text{O}(13)\text{--Mo}^{\text{V}}(4)\text{--O}(6')$ . The simplified neutral fragment (Figure 6) used for the extended-Hückel calculations of the  $\text{Mo}^{\text{V}}(4)$  site provides two minima in the total bonding energy of 57 valence electrons,  $E(2.5, -10)$  and  $E(1.1, -20)$ . However, (2.5, -10) and (1.1, -20) are unfavourable conformations involving strongly asymmetric contributions (Table 5) of the H(13) and H(6') 1s orbitals to the s.o.m.o. In addition, (1.1, -20) is also not the observed conformation, because of the unacceptably short Mo–H distance. As represented in Table 5, a nearly equal contribution of the H(13) and H(6') atoms to the s.o.m.o. is obtained for conformations (1.8, -10) and (1.9, -10), for which the full potential energy surface is a saddle zone (Figure 7). Any other conformations give asymmetric contributions of the two H atoms to the s.o.m.o. A low-temperature neutron-diffraction study of  $[\text{W}(\text{CO})_3(\text{PPR}_3)_2\text{H}_2]$  gave a W–H distance of 1.89 Å.<sup>17</sup> Since the bond energy of Mo–H is smaller than that of W–H,<sup>2,18</sup> the conformation (1.9, -10) can be taken to be more plausible than (1.8, -10). The  $\text{H}(13)\cdots\text{Mo}^{\text{V}}(4)\cdots\text{H}(6')$  direction for (1.9, -10) is inclined at  $31^\circ$  to  $A_{\text{H}1}$  in alternative 1, defining approximately the maximum component vector of the  $A_{\text{H}}$  tensors. The extended-Hückel calculation for (1.9, -10) provides at least three electronic transitions from the s.o.m.o. to the antibonding molecular orbitals (a.m.o.) in the visible and near-i.r. region. The relative energies and predominant atomic orbital coefficients of the four molecular orbitals are shown in Table 6. The computed energy levels for (1.9, -10) can be used to interpret the electronic absorption spectrum observed for the  $\text{Mo}^{\text{V}}(4)$  site [Figure 4(a)]: the electronic transition responsible for the absorption with a large intensity at ca. 490 nm corresponds to the electronically allowed transition s.o.m.o.  $\longrightarrow$  a.m.o.<sub>3</sub> ( $\lambda_{\text{max.}} = 502 \text{ nm}$ ), and the transitions responsible for the shoulder at ca. 800 nm and for a weak absorption at 1 180 nm may be ascribed to the electronic rearrangements s.o.m.o.  $\longrightarrow$  a.m.o.<sub>2</sub> ( $\lambda_{\text{max.}} = 775 \text{ nm}$ ) and  $\longrightarrow$  a.m.o.<sub>1</sub> ( $\lambda_{\text{max.}} = 1 222 \text{ nm}$ ), respectively. As shown in Tables 5 and 6, the s.o.m.o. for

\*  $(A_{\text{H}1}, A_{\text{H}2}, A_{\text{H}3}) = (-8.94, +8.41, +6.78), (-8.94, +8.41, -6.78),$  and  $(-8.94, +8.41, +6.78) \times 10^{-4} \text{ cm}^{-1}$  provide unacceptably large values of the anisotropic tensor compared with the isotropic interaction, considering the hyperfine interactions with the  $\alpha$  proton.<sup>14</sup>

**Table 6.** Computed energy levels (eV) \* and predominant atomic orbital coefficients of the three antibonding molecular orbitals above the s.o.m.o. for conformation (1.9, -10)

		s.o.m.o.	a.m.o. <sub>1</sub>	a.m.o. <sub>2</sub>	a.m.o. <sub>3</sub>
		0	1.0114	1.5982	2.4687
Mo(4)	5s	-0.0719	-0.0644	0.0833	-0.0401
	4d <sub>z<sup>2</sup></sub>	0.2178	0.0971	-0.1188	0.0700
	4d <sub>x<sup>2</sup>-y<sup>2</sup></sub>	0.2678	0.1597	-0.0214	0.2068
	4d <sub>xy</sub>	0.1743	0.8399	-0.0292	-0.1503
	4d <sub>y<sup>2</sup></sub>	-0.5551	0.4134	-0.0023	0.2813
	4d <sub>zx</sub>	0.0432	0.0417	0.9301	0.0495
O(6')	2p <sub>x</sub>	-0.0772	-0.0123	-0.2341	-0.0873
	2p <sub>y</sub>	0.4775	0.1101	-0.0211	0.3354
	2p <sub>z</sub>	-0.0374	0.0322	0.0186	-0.1148
O(9)	2p <sub>x</sub>	-0.0719	-0.0384	0.0309	-0.1179
	2p <sub>z</sub>	0.0653	-0.0243	-0.0223	0.1871
O(12)	2p <sub>y</sub>	0.1780	0.3734	-0.0102	0.0462
	2p <sub>z</sub>	0.0497	0.0217	0.3906	0.0328
O(13)	2s	0.0761	-0.0100	0.0091	-0.1649
	2p <sub>x</sub>	0.0600	0.0149	0.2498	-0.0572
	2p <sub>y</sub>	-0.2689	0.0567	-0.0230	0.2787
	2p <sub>z</sub>	-0.0757	0.0169	0.0424	-0.0854
O(14)	2p <sub>x</sub>	0.0656	0.1888	-0.0485	-0.0119
	2p <sub>y</sub>	-0.0371	-0.0044	0.0435	0.0816
	2p <sub>z</sub>	-0.2341	0.0949	0.0640	0.0658
N(3)	2p <sub>x</sub>	-0.0913	-0.0117	-0.0016	0.0855
	2p <sub>y</sub>	0.1608	0.0218	0.0218	-0.1495
	2p <sub>z</sub>	0.1325	0.0185	0.0032	-0.1243
H(6')	1s	-0.2846	-0.0169	0.0384	-0.6175
H(13)	1s	-0.2161	-0.0353	-0.0051	0.4773

\* Relative to s.o.m.o.

conformation (1.9, -10) consists of the extensively mixed *d* orbitals and a significant contribution from oxygen and nitrogen 2*p* orbitals in addition to Mo 5*s* and H(13) and H(6') 1*s* orbitals. Such an orbital mixing undoubtedly leads to a large isotropic component of *A*<sub>H</sub> tensors (Table 2) and the deviation of the *A*<sub>Mo</sub> anisotropic component from axial symmetry. Although the deviation of *A*<sub>Mo</sub> from the axial symmetry does not necessarily make the point-dipole approximation reasonable, the unpaired electron density (= 1.128) on Mo 4*d* orbitals evaluated by using the dipole approximation for the e.s.r. data is overestimated and in part distributed on O and N 2*p* orbitals, as suggested by the extended-Hückel calculations (Table 5). The mixing between the various molybdenum-based antibonding molecular orbitals (Table 6), which is allowed by the low symmetry, results in the non-coincidence of the principal axes of the *g* and *A*<sub>Mo</sub> tensors (Table 3). Conformation (1.9, -10) represents an O(13)-H(13) distance of 1.43 Å. This is rather long for an O-H bond, and results from the significant mixing of Mo 4*d* and O and N 2*p* orbitals in the s.o.m.o. (Table 5). A similar distance has recently been reported from the single-crystal proton electron nuclear double resonance of  $\gamma$ -irradiated [NH<sub>4</sub>]<sub>6</sub>[Mo<sub>7</sub>O<sub>24</sub>] $\cdot$ 4H<sub>2</sub>O at 15 K:<sup>19</sup> the position of the proton at the Mo<sup>V</sup> site, calculated using the point-dipole approximation, was 1.46 Å from the O atom, which is close to the limits of applicability of the point-dipole approximation. If we recall that the solid-state photochemistry of alkylammonium polyoxomolybdates corresponds to the initial stage of the

solution photochemistry,<sup>5</sup> the (1.9, -10) conformation, characterizing the saddle zone in the full potential energy surface (Figure 7), can be regarded as a transition state for the photoredox reaction in solutions, suggesting that H(13) will be labile enough to transfer to O(14) or N(3) in the solution.<sup>5</sup> Thus, the (1.9, -10) geometry containing 57 valence electrons provides a good qualitative explanation of the e.s.r. data, although the spin densities in the Mo 5*s* and the two H 1*s* orbitals are under- and over-estimated, respectively. One could suggest the fragment containing 56 valence electrons as a better model for the Mo<sup>V</sup>(4) site. This corresponds to a biradical-like electron-hole pair, where the lower orbital made up primarily of O(14), or N(3) 2*s* and 2*p* atomic orbitals is occupied by one electron (hole) instead of two electrons, as suggested in Figure 2. This will result in an increase in *E*(*R*,  $\theta$ ) values. However, the calculations revealed no significant difference in the *E*(*R*,  $\theta$ ) curves (Figure 7).

## References

- 1 T. Yamase, *Polyhedron*, 1986, 5, 79.
- 2 T. Yamase, *J. Chem. Soc., Dalton Trans.*, 1987, 1597.
- 3 T. Yamase and T. Usami, *J. Chem. Soc., Dalton Trans.*, 1988, 183.
- 4 T. Yamase, *J. Chem. Soc., Dalton Trans.*, 1978, 283.
- 5 T. Yamase, R. Sasaki, and T. Ikawa, *J. Chem. Soc., Dalton Trans.*, 1981, 628.
- 6 T. Yamase, *J. Chem. Soc., Dalton Trans.*, 1982, 1987.
- 7 T. Yamase, *J. Chem. Soc., Dalton Trans.*, 1985, 2585.

- 8 Y. Sasaki, T. Yamase, Y. Ohashi, and Y. Sasada, *Bull. Chem. Soc. Jpn.*, 1987, **60**, 4285.
- 9 M. Isobe, F. Marumo, T. Yamase, and T. Ikawa, *Acta Crystallogr., Sect. B*, 1978, **34**, 2728.
- 10 T. Yamase and T. Ikawa, *Bull. Chem. Soc. Jpn.*, 1977, **50**, 746.
- 11 R. Hoffmann, *J. Chem. Phys.*, 1963, **39**, 1397; J. H. Ammeter, H-B. Bürgi, J. C. Thibeault, and R. Hoffmann, *J. Am. Chem. Soc.*, 1978, **100**, 3686; R. A. Wheeler, M-H. Whangbo, T. Hughbands, R. Hoffmann, J. K. Burdett, and T. A. Albright, *ibid.*, 1986, **108**, 2222.
- 12 'International Tables for X-Ray Crystallography,' D. Reidel, Dordrecht, Boston, Lancaster, Tokyo, 1985, vol. 4, p. 267.
- 13 J. R. Morton and K. F. Preston, *J. Magn. Reson.*, 1978, **30**, 577.
- 14 J. R. Morton, *Chem. Rev.*, 1964, **64**, 453.
- 15 L. Pauling, 'The Nature of the Chemical Bond,' Cornell University Press, Ithica, New York, 1948, p. 70.
- 16 D. Polley and D. H. Whiffen, *Trans. Faraday Soc.*, 1961, **57**, 1445; W. Derbyshire, *Mol. Phys.*, 1962, **5**, 225.
- 17 G. K. Kubas and R. R. Ryan, *Polyhedron*, 1986, **5**, 473.
- 18 R. G. Pearson, *Chem. Rev.*, 1985, **85**, 41; R. J. Klinger, J. C. Huffman, and J. K. Kochi, *J. Am. Chem. Soc.*, 1980, **102**, 208.
- 19 N. M. Atherton and R. D. S. Blackford, *Mol. Phys.*, 1987, **61**, 443.

Received 31st May 1988; Paper 8/02149J